




Cite this: *Mater. Adv.*, 2020,
1, 3256

Multiplex surface-enhanced Raman scattering detection of deoxynivalenol and ochratoxin A with a linear polymer affinity agent†

Rebeca S. Rodriguez,  Victoria M. Szlag, Theresa M. Reineke  and
Christy L. Haynes *

A linear, methacrylamide polymer affinity agent was explored to capture two mycotoxins, deoxynivalenol (DON) and ochratoxin A (OTA), for multiplex surface-enhanced Raman scattering (SERS) detection. These mycotoxins are naturally occurring small molecules from fungi that can be dangerous at low concentrations. SERS detection was completed for each polymer-toxin complex at concentrations relevant to current safety regulation by the FDA: 1 ppm for DON and 5 ppb for OTA. Visibly distinguishable vibrational modes were observed in the multiplex spectra that were attributed to each mycotoxin individually, thus, not requiring any additional chemometric analysis. Density functional theory (DFT) was used to model DON and OTA to accurately label the vibrational modes in the experimental spectra as well as provide insight on the binding between both targets and the affinity agent. Fully modeled vibrations of these toxins are novel contributions due to OTA never being modeled and there being only a few published vibrational modes of DON. DFT guides empirical observations regarding hydrogen bonding at multiple sites of each mycotoxin target molecule through the amine groups on the polymer, confirming the capabilities of a single polymer affinity agent to facilitate multiplex detection of a class of molecules through less-specific interactions than traditional affinity agents.

Received 15th August 2020,
Accepted 25th October 2020

DOI: 10.1039/d0ma00608d

rsc.li/materials-advances

Introduction

Polymers can serve as affinity agents to capture and detect a wide variety of analytes. Synthetic affinity agents are compelling because they are relatively inexpensive and robust, and can be easily synthesized to tune and exploit certain interactions. Whether in conjunction with other affinity agents for increased specificity¹ or synthesized specifically to bind to a target,² these agents can be used to identify and detect biological toxins,³ food contaminants,⁴ and other small molecules.⁵ Polymeric molecularly imprinting (immobilizing a target as a template in a polymer matrix) has long served as the synthetic mechanism to generate polymer-based affinity agents for sensors. However, these systems are difficult to characterize and reproduce, due to their insoluble nature, and sensing measurements have not been directly made in a complex matrix.^{6–8} In addition, because they are cast to bind a specific target, they cannot detect multiple targets at once without adding additional synthetic steps. These relatively thick polymer templates make

it difficult to use surface analytical techniques for target detection due to the fact that the majority of the sensing volume is occupied by the polymer matrix rather than the matrix with captured analytes.

In contrast, linear polymer affinity agents allow one to synthetically control the chain length of the polymer and multivalent display of functional groups, where each monomer repeat unit serves as a potential binding site for the target analyte.^{9,10} Previous work by Szlag and coauthors¹¹ designed a single-point-attachment polymer affinity agent with pendant saccharide moieties on the repeat unit structure to specifically bind a protein used as a bioterror agent. Leveraging simple chemistry with an attractive analytical technique like surface-enhanced Raman scattering (SERS), one can monitor binding of the target to the polymer in both purified and complex matrices. Expanding on this concept, if one allows for similar bonding interactions, the choice of the polymer repeat unit can facilitate multiplex capture of an entire class of molecules.

In light of multiplex detection, SERS is a particularly useful signal transduction mechanism because of its low limits of detection, its ability to provide a spectral “fingerprint” unique to the analyte of interest, and its compatibility with aqueous samples.^{9,12,13} When an analyte is immobilized near a plasmonic metal surface, one can observe an enhanced intensity of the

Department of Chemistry, University of Minnesota, 207 Pleasant Street SE,
Minneapolis, Minnesota 55455, USA. E-mail: chaynes@umn.edu

† Electronic supplementary information (ESI) available: Vibrational band assignments for each mycotoxin, spectra of each mycotoxin without an affinity agent, and isothermal titration calorimetry studies. See DOI: 10.1039/d0ma00608d



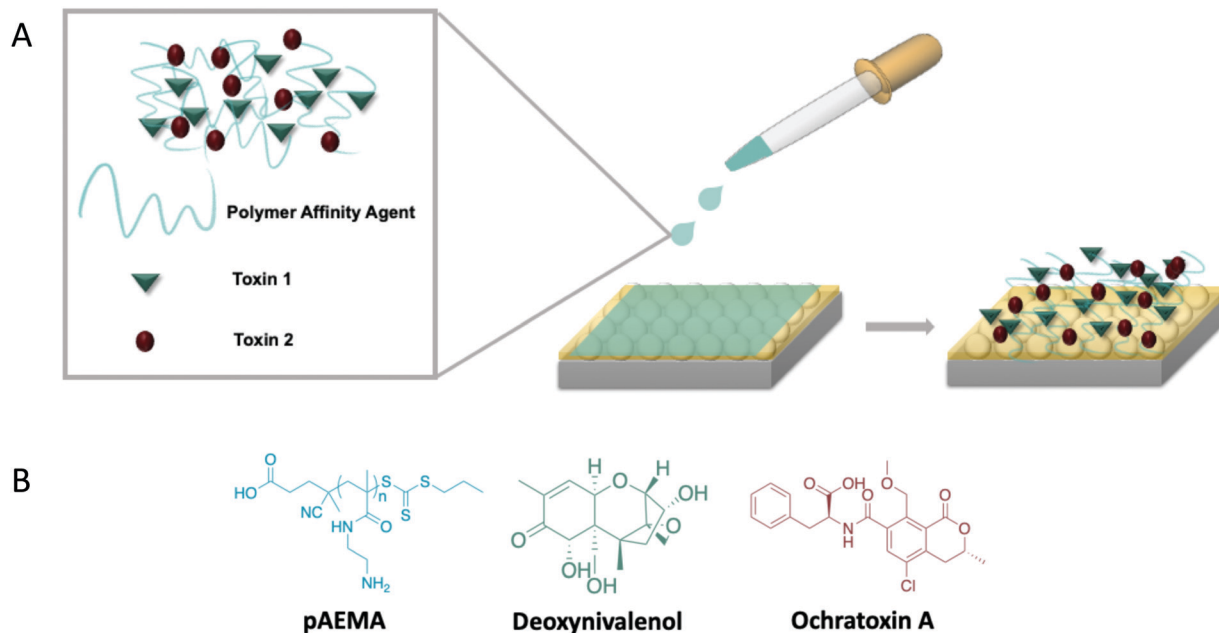


Fig. 1 Illustrative image of multiplex detection on film over nanospheres (FON) SERS substrates. (A) Image of in-solution interactions occurring with a polymer affinity agent and two small molecule toxins. The then complexed molecules attach onto the gold FON surface. (B) Molecular structures for the methacrylamide polymer (pAEMA) and two small molecule toxins used in this study (deoxynivalenol and ochratoxin A).

ambient air. The mixture was dialyzed in a 100–500 Da MWCO membrane against 3 L of Milli-Q water for 24 h. This was then lyophilized, resulting in a dry, light yellow solid with a yield of 78%. The polymer molecular weight was characterized *via* aqueous mobile phase (0.1 M Na₂SO₄ in 1.0 vol% acidic acid) size exclusion chromatography (SEC). The instrument used was an Agilent 1260 Infinity Quaternary LC System with Eprogen columns [CATSEC1000 (7 μm, 50 × 4.6), CATSEC100 (5 μm, 250 × 4.6), CATSEC300 (5 μm, 250 × 4.6), and CATSEC1000 (7 μm, 250 × 4.6)]. The system was equipped with a Wyatt HELEOS II light scattering detector ($\lambda = 662$ nm) and an Optilab rEX refractometer ($\lambda = 658$ nm). The SEC traces are shown in the ESI† (Fig. S1).

Isothermal titration calorimetry (ITC)

ITC measurements were performed using a MicroCal PEAQ-ITC Automated (Malvern Instruments, Westborough, MA) at 25 °C as previously discussed in previous literature.^{15,16} The sample cell and injection syringe were cleaned with 20% Contrad 70 detergent, water, and methanol. The instrument syringe was flushed with 10% bleach twice after each experiment. A 22 vol% DMSO, 16 vol% methanol, 62 vol% acetate buffer (pH 5) mixture was used to make a 4.0 mM polymer repeat unit solution and 0.26 mM OTA and DON samples. The instrument automatically transferred polymer into the mycotoxin samples (or into blank solvent for the background titration). The titration uses a 1.5 μL injection volume and 150 s injection intervals. Raw ITC profiles (Fig. S2a and b, ESI†) are measured as heat flow rate against time where each peak refers to the injected sample. Integration of these peaks, with respect to time, produces the final ITC plot depicting total heat absorption

at each injection *vs.* polymer repeat unit (RU)/toxin ratio (Fig. S2c, ESI†).

Film over nanosphere (FON) fabrication and characterization

FONs were fabricated as previously reported in literature.^{16,27,44} 590 nm-diameter silica nanospheres were dropcast on 1 cm × 1 cm silicon wafers to form a nanosphere mask. A 95.3 nm pure gold film was deposited under vacuum, measured by a quartz crystal microbalance (Denton Vacuum, Moorestown, NJ). FONs with a localized surface plasmon resonance (LSPR) λ_{max} between 750 and 850 nm, measured using a fiber optic probe (Ocean Optics, Dunedin, Florida) with a flat gold film as the reflective standard, were used for these studies.

Surface-enhanced Raman scattering (SERS)

A 1 mM polymer solution (40 : 60 MeOH/water) was mixed with 50% by volume solutions of varying concentrations of DON and OTA and left to interact for 6 h. FON substrates were then incubated in 200 μL of the complexed mixture in a 24-wellplate for 18 h. Substrates were then washed with 1–2 mL of Milli-Q water and air dried. Measurements were performed using a Snowy Range Instruments SnRI ORS System with a 785 nm laser, 9 mW incident power, and a 10 s integration time. Each condition was measured on three substrates, and five spots on each substrate was measured for a total of 15 averaged spectra. The FON average spectrum was baselined in OriginLab's Origin 9.1 (using eleven anchor points created by the first and second derivative with a Savitsky–Golay smoothing and connected by B-spline interpolation, with the same number of points as the input spectrum) and normalized by the incident power and integration time.



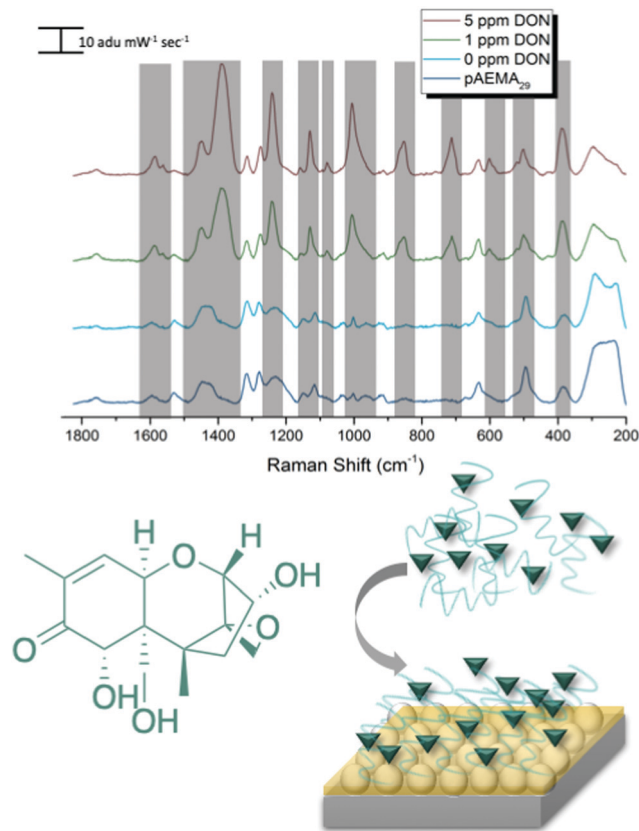


Fig. 3 Experimental spectra of DON and pAEMA₂₉ complex at varying concentrations of DON. Each spectrum is an average of 15 spectra captured in the same conditions. The grey boxes highlight any spectral changes seen different from that of the control spectra.

computational spectrum, the monomer/CTA spectrum, and the experimental spectra, we can further confirm binding between small molecule and polymer. A comparison of DON and monomer/CTA DFT vibrational modes to experimental vibrational modes can be seen in Table 1. A graph displaying SERS

intensity as it relates to DON concentration at a specific wavenumber shift can be seen in Fig. S7 (ESI†).

SERS detection of ochratoxin A with pAEMA₂₉

Following the same protocol as with DON, FONs were incubated in an OTA and pAEMA₂₉ mixture at varying concentrations, and the captured spectra can be seen in Fig. 4. Distinct and visible spectral changes are observed at concentrations as low as the OTA regulatory limit (0.005 ppm/5 ppb). A select table comparing OTA

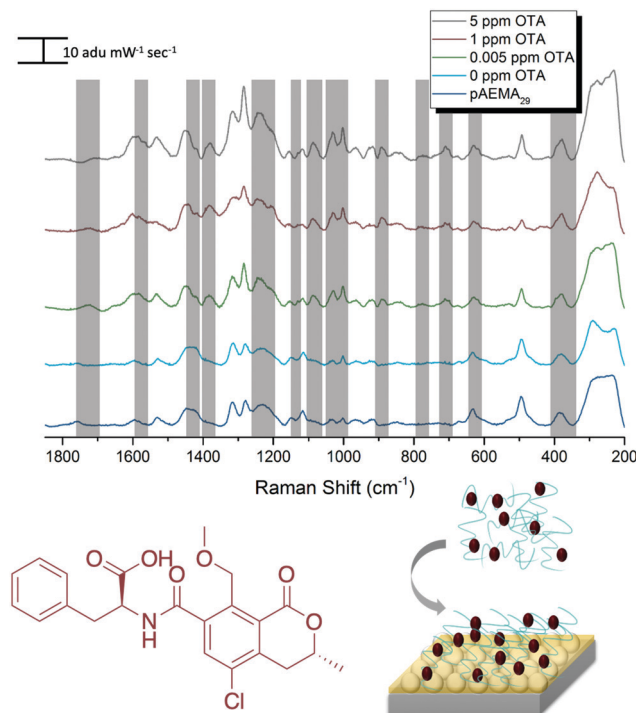


Fig. 4 Experimental spectra of OTA and pAEMA₂₉ complex at varying concentrations of OTA. Each spectrum is an average of 15 spectra captured in the same conditions. The grey boxes highlight any spectral changes seen different from that of the control spectra.

Table 1 Table of select vibrational modes comparing computational DON and monomer/CTA to experimental spectra

DON DFT calculated Raman shift (cm ⁻¹ shift)	DON experimental Raman shift (cm ⁻¹ shift)	Monomer/CTA calculated Raman shift (cm ⁻¹ shift)	Monomer/CTA experimental Raman shift (cm ⁻¹ shift)
1530: scissoring of H's on C12, twisting of H's on C15	1590 and 1566 shoulder	1610: monomer bending of N2 H's	1607
1450: asymmetric out of plane rocking of H's on C17 and wagging of H38 on O5, wagging of H37 on O4, slight wagging of H's on C11	1455	1423 and 1428: O1-C4-N1 symmetric stretch, N1-C5 stretch, rocking of H on N1 and asymmetric bending of C1 H's respectively	1433
1384: rocking of H37 on O4, symmetric angle bending of C18-C14 displacing H35 and H28, rocking of Hs on C21, ring rocking of cyclohexene	1388		
1245: strong stretching of H22 on C10, symmetric stretching of H27 on C13 and O3 on C13, strong angle wagging of H38 on O5 and H33 on C17	1241	1238: twisting/wagging of H's on N1, C5, C6, and N2	1234
853: ring breathing C10, H's on C11 in plane stretch, H32 rocking, H35 bend	852		



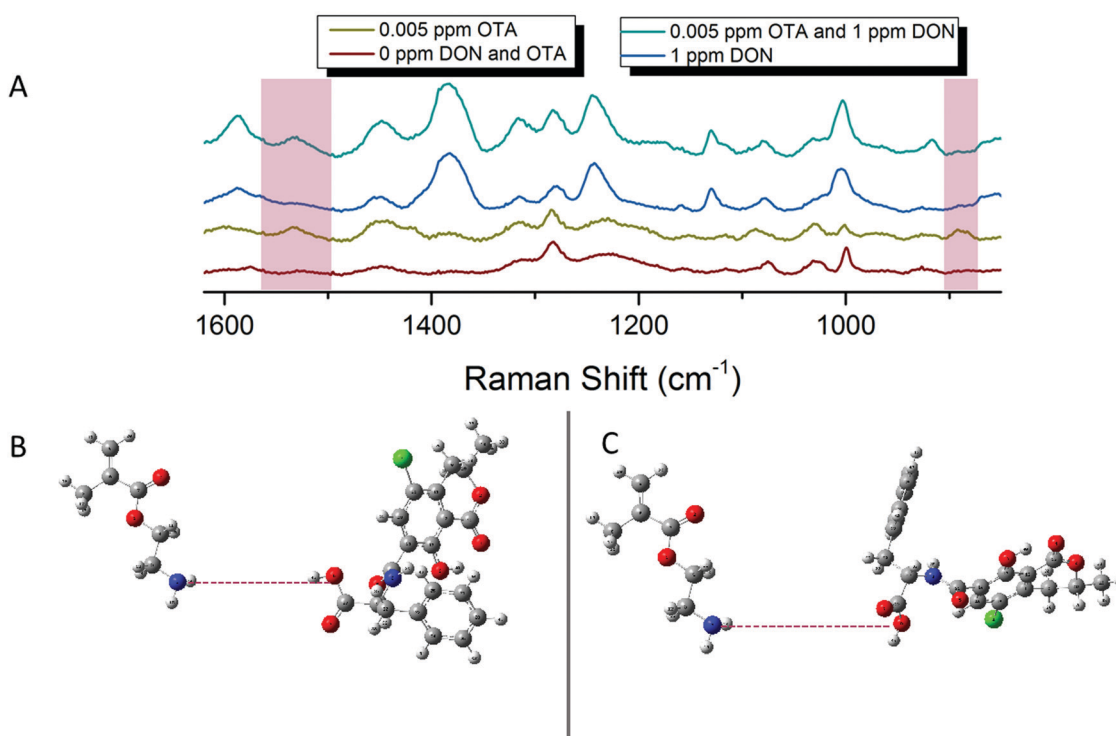


Fig. 6 (A) Enlarged multiplex spectra highlighting the OTA stand-alone peaks. (B) Hypothesized interactions between AEMA monomer and OTA at 1535 cm^{-1} shift based on vibrational animations in Gaussian. (C) Hypothesized interactions between AEMA monomer and OTA at 916 cm^{-1} shift based on vibrational animations in Gaussian.

time, the stretch is attributed to strong vibrations on the benzyl ring of the phenylalanine moiety of OTA. This indicates hydrogen bonding at the carboxyl of the OTA phenylalanine. The second stand-alone peak in the multiplex spectra, at 916 cm^{-1} shift, can be referenced to the 917 cm^{-1} shift in the computational spectrum due to strong asymmetric stretching of the tertiary carbons attached to the carboxyl group previously mentioned. This further confirms hydrogen bonding between OTA and the linear polymer affinity agent. An enlarged image of the multiplex spectra and hypothesized binding can be seen in Fig. 6.

Following the same hypotheses for OTA and pAEMA₂₉, observing the unique DON peaks in the multiplex spectra, can help reveal molecular details about DON interactions with the polymer affinity agent. The peak at 1455 cm^{-1} shift in the multiplex spectra can be referenced to 1450 cm^{-1} shift from the computational spectrum, strong asymmetric rocking of the hydrogens on a tertiary carbon bound to a hydroxyl group, indicating hydrogen bonding at the hydroxyl. At 1234 cm^{-1} shift, the polymer and blank spectra have a broadened peak that shifts and sharpens into a peak at 1241 cm^{-1} shift that can be referenced to the 1245 cm^{-1} shift in the computational spectrum of DON. This vibrational mode is attributed to both strong stretching of the hydrogens on the bicyclic ring near the hydroxyl (O3) and symmetric stretching of the hydrogens in the out-of-plane hydroxyl group (O5) as labeled in Fig. 7. Lastly, the sharp 1130 cm^{-1} shift band of DON in the multiplex spectra can be referenced to strong stretches at 1142 and 1146 cm^{-1}

shifts in the computational spectrum. These strong vibrations are due to hydrogen stretches on the bicyclic ring near the hydroxyl (O3), with movement in the epoxide ring and symmetric stretching in the epoxide ring hydrogens with symmetric stretching of the hydrogens in the out-of-plane hydroxyl group (O5), respectively as labeled in Fig. 7D and E. While full analysis of OTA and DON with pAEMA in a food matrix is out of the scope of this work, we have included a spectra of wheat beer on bare FON (Fig. S10, ESI†). We predict that we will be able to observe DON and OTA character in this complex matrix because of the position of the multiplex vibrational modes when compared to the beer signature. There are no visible peaks at 916 cm^{-1} shift (OTA), 1130 cm^{-1} shift (DON), or 1234 cm^{-1} shift (DON) in the beer only spectra, setting precedent for the ability to multiplex in the complex media these toxins contaminate.

Conclusions

Here we have exploited the use of basic molecular hypotheses to design a linear polymer affinity agent that can bind multiple targets. pAEMA, a simple and inexpensive linear polymer, can be used to complex at least two small molecule mycotoxins, DON and OTA, and anchor onto a sensing substrate through trithiocarbonate and gold interactions. We have shown that we can detect both toxins individually using SERS, with no additional sensing probe molecule. Sensing of both toxins



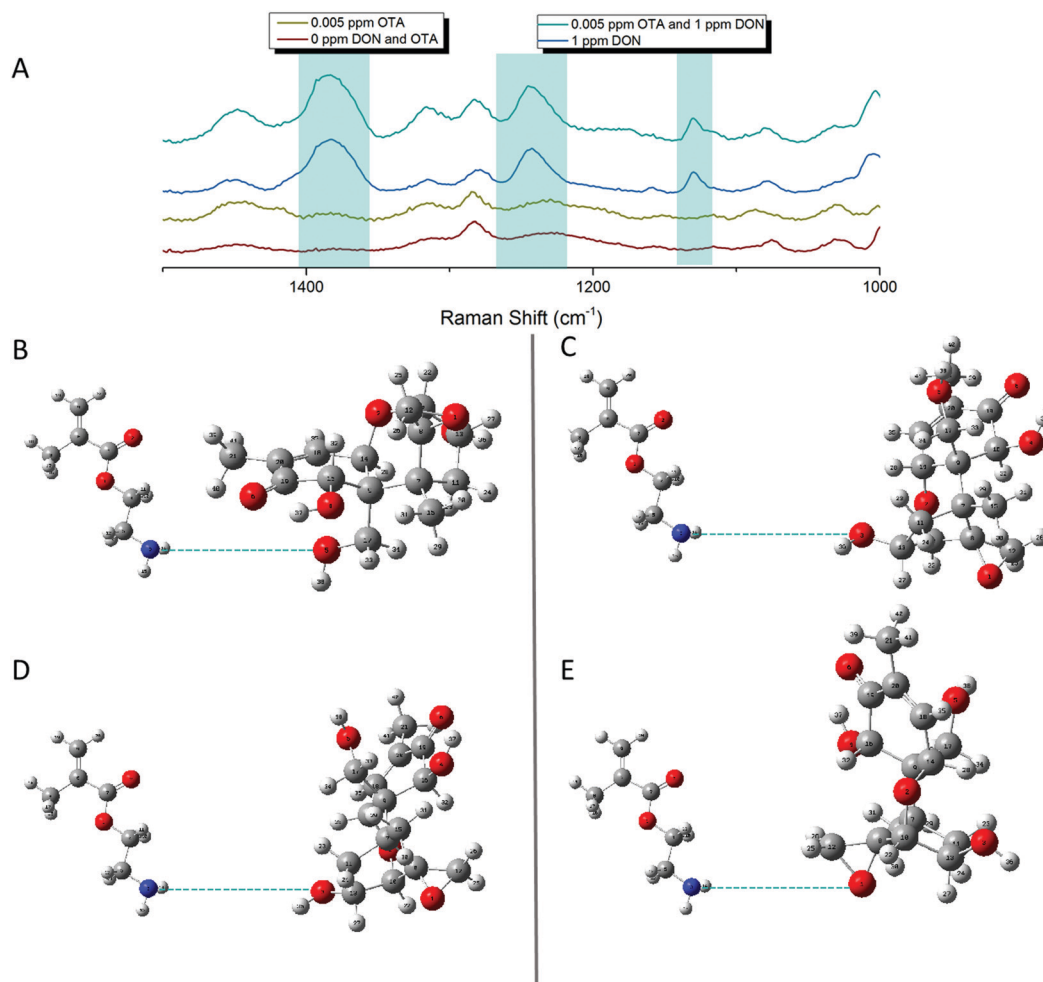


Fig. 7 (A) Enlarged multiplex spectra highlighting the DON stand-alone peaks. (B) Hypothesized interactions between AEMA monomer and DON at 1450 cm^{-1} shift and 1245 cm^{-1} shift based on vibrational animations in Gaussian. (C) Second hypothesized interactions between AEMA monomer and DON at 1245 cm^{-1} based on vibrational animations in Gaussian. (D and E) Hypothesized interactions between AEMA monomer and DON at 1142 cm^{-1} and 1145 cm^{-1} shift based on vibrational animations in Gaussian.

simultaneously is possible and visibly distinguishable without any chemometric analysis of the data. We have computationally modeled the OTA Raman spectrum for the first time as well as added to the overall vibrational labeling of the DON Raman spectrum. Moreover, DFT can assist not only in the labeling of strong vibrational modes, but in the ability to monitor the stretches in real-time, allowing us to make clear conclusions about the fundamental interactions occurring between target and affinity agent during sensing. Through this work, we have noted that hydrogen bonding associates the two mycotoxins to the polymer through the amine groups. Additionally, there seems to be hydrogen bonding occurring at multiple sites on the small molecules based on the location of the vibrational shifts. Both toxins are able to interact and complex to the polymer at concentrations relevant to their regulation limits: 1 ppm and 5 ppb for DON and OTA, respectively. This further shows that linear polymer affinity agents can serve as unique capture agents due to their easily modifiable pendant groups, inexpensive nature, and non-specificity towards solely one target. We note that any properties, physical or chemical, that

change the overall polymer will impact the polymer's ability to act as an effective affinity agent. However, these changes may promote reversibility of the sensor in future work. Future work will explore their use in complex matrices that are relevant to these targets in order to make this a commercially viable sensing system as well as continued optimization of the sensing substrates to facilitate relatively fast and efficient multiplex sensing.

Author contributions

The manuscript was written through contributions of all authors. All authors have given approval to the final version of the manuscript.

Funding sources

Isothermal titration calorimetry was carried out using an ITC-200 microcalorimeter, funded by the NIH Shared Instrumentation



Grant S10-OD017982. RSR would like to acknowledge both the Mistletoe Foundation and the Lester C. and Joan M. Krogh Endowed Fellowship through the Chemistry department of UMN for funding.

Conflicts of interest

The authors have no conflicts to declare.

Acknowledgements

We would like to acknowledge 3M for their collaboration and funding and the Minnesota Super Computing Institute for their facilities. RSR would like to acknowledge both the Mistletoe Foundation and the Lester C. and Joan M. Krogh Endowed Fellowship through the Chemistry department of UMN for funding. RSR would also like to thank Daniel Graham from the Goodpaster Group and members of the Reineke group, specifically Derek Saxon and Rishad Dalal, for their thoughtful discussions.

Notes and references

- N. Malmstadt, D. E. Hyre, Z. Ding, A. S. Hoffman and P. S. Stayton, Affinity Thermoprecipitation and Recovery of Biotinylated Biomolecules *via* a Mutant Streptavidin–Smart Polymer Conjugate, *Bioconjugate Chem.*, 2003, **14**(3), 575–580, DOI: 10.1021/bc020055l.
- J. Xu, S. Ambrosini, E. Tamahkar, C. Rossi, K. Haupt and B. Tse Sum Bui, Toward a Universal Method for Preparing Molecularly Imprinted Polymer Nanoparticles with Antibody-like Affinity for Proteins, *Biomacromolecules*, 2016, **17**(1), 345–353, DOI: 10.1021/acs.biomac.5b01454.
- A. Ait Lahcen, F. Arduini, F. Lista and A. Amine, Label-Free Electrochemical Sensor Based on Spore-Imprinted Polymer for *Bacillus Cereus* Spore Detection, *Sens. Actuators, B*, 2018, **276**, 114–120, DOI: 10.1016/j.snb.2018.08.031.
- H. Munawar, K. Smolinska-Kempisty, A. Garcia Cruz, F. Canfarotta, E. Piletska, K. Karim and S. A. Piletsky, Molecularly Imprinted Polymer Nanoparticle-Based Assay (MINA): Application for Fumonisin B1 Determination, *Analyst*, 2018, **143**(14), 3481–3488, DOI: 10.1039/C8AN00322J.
- C. S. Storer, Z. Coldrick, D. J. Tate, J. M. Donoghue and B. Grieve, Towards Phosphate Detection in Hydroponics Using Molecularly Imprinted Polymer Sensors, *Sensors*, 2018, **18**(2), 531, DOI: 10.3390/s18020531.
- J. J. BelBruno, Molecularly Imprinted Polymers, *Chem. Rev.*, 2019, **119**(1), 94–119, DOI: 10.1021/acs.chemrev.8b00171.
- J. O. Mahony, K. Nolan, M. R. Smyth and B. Mizaikoff, Molecularly Imprinted Polymers—Potential and Challenges in Analytical Chemistry, *Anal. Chim. Acta*, 2005, **534**(1), 31–39, DOI: 10.1016/j.aca.2004.07.043.
- G. Vasapollo, R. D. Sole, L. Mergola, M. R. Lazzoi, A. Scardino, S. Scorrano and G. Mele, Molecularly Imprinted Polymers: Present and Future Prospective, *Int. J. Mol. Sci.*, 2011, **12**(9), 5908–5945, DOI: 10.3390/ijms12095908.
- V. M. Szlag, R. S. Rodriguez, J. He, N. Hudson-Smith, H. Kang, N. Le, T. M. Reineke and C. L. Haynes, Molecular Affinity Agents for Intrinsic Surface-Enhanced Raman Scattering (SERS) Sensors, *ACS Appl. Mater. Interfaces*, 2018, **10**(38), 31825–31844, DOI: 10.1021/acsami.8b10303.
- J. Lee, J. W. Sohn, Y. Zhang, K. W. Leong, D. Pisetsky and B. A. Sullenger, Nucleic Acid-Binding Polymers as Anti-Inflammatory Agents, *Proc. Natl. Acad. Sci. U. S. A.*, 2011, **108**(34), 14055–14060, DOI: 10.1073/pnas.1105777108.
- V. M. Szlag, M. J. Styles, L. R. Madison, A. R. Campos, B. Wagh, D. Sprouse, G. C. Schatz, T. M. Reineke and C. L. Haynes, SERS Detection of Ricin B-Chain *via* N-Acetyl-Galactosamine Glycopolymers, *ACS Sens.*, 2016, **1**(7), 842–846, DOI: 10.1021/acssensors.6b00209.
- C. L. Haynes, A. D. McFarland and R. P. Van Duyne, Surface-Enhanced Raman Spectroscopy, *Anal. Chem.*, 2005, **77**(17), 338A–346A, DOI: 10.1021/ac053456d.
- K. C. Bantz, A. F. Meyer, N. J. Wittenberg, H. Im, Ö. Kurtuluş, S. H. Lee, N. C. Lindquist, S.-H. Oh and C. L. Haynes, Recent Progress in SERS Biosensing, *Phys. Chem. Chem. Phys.*, 2011, **13**(24), 11551–11567, DOI: 10.1039/C0CP01841D.
- K. M. Mayer and J. H. Hafner, Localized Surface Plasmon Resonance Sensors, *Chem. Rev.*, 2011, **111**(6), 3828–3857, DOI: 10.1021/cr100313v.
- V. M. Szlag, S. Jung, R. S. Rodriguez, M. Bourgeois, S. Bryson, G. C. Schatz, T. M. Reineke and C. L. Haynes, Isothermal Titration Calorimetry for the Screening of Aflatoxin B1 Surface-Enhanced Raman Scattering Sensor Affinity Agents, *Anal. Chem.*, 2018, **90**(22), 13409–13418, DOI: 10.1021/acs.analchem.8b03221.
- V. M. Szlag, R. S. Rodriguez, S. Jung, M. R. Bourgeois, S. Bryson, A. Purchel, G. C. Schatz, C. L. Haynes and T. M. Reineke, Optimizing Linear Polymer Affinity Agent Properties for Surface-Enhanced Raman Scattering Detection of Aflatoxin B1, *Mol. Syst. Des. Eng.*, 2019, **4**, 1019–1031, DOI: 10.1039/C9ME00032A.
- A. R. Campos, Z. Gao, M. G. Blaber, R. Huang, G. C. Schatz, R. P. Van Duyne and C. L. Haynes, Surface-Enhanced Raman Spectroscopy Detection of Ricin B Chain in Human Blood, *J. Phys. Chem. C*, 2016, **120**(37), 20961–20969, DOI: 10.1021/acs.jpcc.6b03027.
- J. Chen, B. Park, Y. Huang, Y. Zhao and Y. Kwon, Label-Free SERS Detection of *Salmonella Typhimurium* on DNA Aptamer Modified AgNR Substrates, *J. Food Meas. Charact.*, 2017, **11**(4), 1773–1779, DOI: 10.1007/s11694-017-9558-6.
- J. W. Bennett and M. Klich, Mycotoxins, *Clin. Microbiol. Rev.*, 2003, **16**(3), 497–516, DOI: 10.1128/CMR.16.3.497-516.2003.
- D. Milicevic, K. Nesic and S. Jaksic, Mycotoxin Contamination of the Food Supply Chain - Implications for One Health Programme, *Procedia Food Sci.*, 2015, **5**, 187–190, DOI: 10.1016/j.profoo.2015.09.053.
- R. a. Gonçalves, D. Schatzmayr, U. Hofstetter and G. Santos, a. Occurrence of Mycotoxins in Aquaculture: Preliminary



- 47 H. Wei, A. McCarthy, J. Song, W. Zhou and P. J. Vikesland, Quantitative SERS by Hot Spot Normalization – Surface Enhanced Rayleigh Band Intensity as an Alternative Evaluation Parameter for SERS Substrate Performance, *Faraday Discuss.*, 2017, **205**, 491–504, DOI: 10.1039/c7fd00125h.
- 48 J. Cao, C. Lu, J. Zhuang, M. Liu, X. Zhang, Y. Yu and Q. Tao, Multiple Hydrogen Bonding Enables the Self-Healing of Sensors for Human–Machine Interactions, *Angew. Chem., Int. Ed.*, 2017, **56**(30), 8795–8800, DOI: 10.1002/anie.201704217.
- 49 J. Zhou, H. Lin, X.-F. Cheng, J. Shu, J.-H. He, H. Li, Q.-F. Xu, N.-J. Li, D.-Y. Chen and J.-M. Lu, Ultrasensitive and Robust Organic Gas Sensors through Dual Hydrogen Bonding, *Mater. Horiz.*, 2019, **6**(3), 554–562, DOI: 10.1039/C8MH01098F.
- 50 E. Piletska, K. Karim, R. Coker and S. Piletsky, Development of the Custom Polymeric Materials Specific for Aflatoxin B1 and Ochratoxin A for Application with the ToxiQuant T1 Sensor Tool, *J. Chromatogr. A*, 2010, **1217**(16), 2543–2547, DOI: 10.1016/j.chroma.2009.11.091.

